Transverse instability and perpendicular electric field in two-dimensional electron phase-space holes

Mingyu Wu,[1,2] Quanming Lu,[1,2] Can Huang,[1] and Shui Wang[1]

Received 28 December 2009; revised 2 July 2010; accepted 6 July 2010; published 26 October 2010.

[1] A multidimensional electron phase-space hole (electron hole) is considered to be unstable to the transverse instability. In this paper, we perform two-dimensional (2D) particle-in-cell (PIC) simulations to study the evolution of electron holes at different plasma conditions; we find that the evolution is determined by combined actions between the transverse instability and the stabilization by the background magnetic field. In very weakly magnetized plasma ($\Omega_e \ll \omega_{pe}$, where Ω_e and ω_{pe} are the electron gyrofrequency and plasma frequency, respectively), the transverse instability dominates the evolution of the electron holes. The parallel cut of the perpendicular electric field ($E_\perp$) has bipolar structures, accompanied by the kinking of the electron holes. Such structures last for only tens of electron plasma periods. With the increase of the background magnetic field, the evolution of the electron holes becomes slower. The bipolar structures of the parallel cut of $E_\perp$ in the electron holes can evolve into unipolar structures. In very strongly magnetized plasma ($\Omega_e \gg \omega_{pe}$), the unipolar structures of the parallel cut of $E_\perp$ can last for thousands of electron plasma periods. At the same time, the perpendicular electric field ($E_\perp$) in the electron holes can also influence electron trajectories passing through the electron holes, which results in variations of charge density along the direction perpendicular to the background magnetic field outside of the electron holes. When the amplitude of the electron hole is sufficiently strong, streaked structures of $E_\perp$ can be formed outside of the electron holes, which then emit electrostatic whistler waves because of the interactions between the streaked structures of $E_\perp$ and vibrations of the kinked electron holes.

Citation: Wu, M., Q. Lu, C. Huang, and S. Wang (2010), Transverse instability and perpendicular electric field in two-dimensional electron phase-space holes, *J. Geophys. Res.*, *115*, A10245, doi:10.1029/2009JA015235.

1. Introduction

[2] Since electron phase-space holes (electron holes) were firstly observed in the Earth's magnetotail with the GEOTAIL satellite [*Matsumoto et al.*, 1994], their existence has further been confirmed in different space environments, such as the auroral region [*Ergun et al.*, 1998a], the transition region of the bow shock [*Bale et al.*, 1998], the solar wind [*Mangeney et al.*, 1999], the magnetopause [*Cattell et al.*, 2002], and the magnetosheath [*Pickett et al.*, 2004]. Electron holes are considered to be stationary Bernstein-Greene-Kruskal (BGK) solutions of the Vlasov and Poisson equations [*Bernstein et al.*, 1957; *Muschietti et al.*, 1999; *Chen et al.*, 2005; *Ng and Bhattacharjee*, 2005]. Electron holes have also been observed in laboratory plasma, for example, in a magnetized plasma surrounded by a waveguide [*Saeki et al.*, 1979], and in an unmagnetized laser-generated plasma [*Sarri et al.*, 2010]. They are positive potential pulses, and the parallel cut of their parallel electric field ($E_\parallel$) has bipolar structures. *Roberts et al.* [1967] proposed that electron holes can be formed out of electron bistream instabilities. Particle-in-cell (PIC) simulations have confirmed that electron holes can be formed during the nonlinear evolution of electron bistream instabilities [*Morse and Nielson*, 1969], and these holes can persist for a sufficiently long time in one-dimensional (1D) PIC simulations [*Omura et al.*, 1994; *Mottez et al.*, 1997; *Lu et al.*, 2005a, 2005b]. These electron beams may be generated in a region with sudden changes of an electrostatic potential, such as a double layer [*Newman et al.*, 2001a] or a shock [*Bale et al.*, 1998]. Multidimensional simulations of bistream instabilities showed that a strong magnetic field or oblique modes are beneficial for the formation of electron holes [*Oppenheim et al.*, 1999; *Amano and Hoshino*, 2009; *Bret et al.*, 2006].

[3] However, the parallel cut of the perpendicular electric field ($E_\perp$) in electron holes has been observed by the Polar and Fast Auroral Snapshot (FAST) satellites to have unipolar structures [*Ergun et al.*, 1998a, 1998b; *Franz et al.*, 1998, 2005; *Grabbe and Menietti*, 2006], and such unipolar structures of $E_\perp$ can also form during the nonlinear evolution

[1]CAS Key Laboratory of Basic Plasma Physics, School of Earth and Space Sciences, University of Science and Technology of China, Hefei, China.
[2]State Key Laboratory of Space Weather, Chinese Academy of Sciences, Beijing, China.

0148-0227/10/2009JA015235

of electron bistream instabilities [*Oppenheim et al.*, 1999]. Recently, *Lu et al.* [2008] proposed a generation mechanism for the unipolar structures of $E_\perp$ in electron holes. Using two-dimensional (2D) electrostatic PIC simulations, *Lu et al.* [2008] demonstrated that electron holes can be formed during the nonlinear evolution of electron bistream instabilities. In these holes, the parallel cut of $E_\parallel$ has a bipolar structure, while the parallel cut of $E_\perp$ has a unipolar structure. Such unipolar structures of $E_\perp$ in electron holes are considered to be combined actions of the transverse instability and the stabilization by the background magnetic field. The transverse instability in electron holes proposed by *Muschietti et al.* [2000] is due to the dynamics of the electrons trapped in the electron holes and is a self-focusing type of instability. Perturbations in electron holes can produce transverse gradients of the electric potential. Such transverse gradients focus the trapped electrons into regions that already have a surplus of electrons, which results in larger transverse gradients and more focusing until the transverse instability finally occurs. Such a process has also been confirmed by self-consistent PIC simulations in *Muschietti et al.* [2000]. In this paper, we perform 2D electrostatic PIC simulations to investigate the evolution of two-dimensional electron holes at different plasma conditions, with an emphasis on the structures of the perpendicular electric field ($E_\perp$) and the generation mechanism of electrostatic whistler waves. The electrostatic whistler waves are often observed in 2D PIC simulations of electron bistream instabilities [*Goldman et al.*, 1999; *Oppenheim et al.*, 1999; *Lu et al.*, 2008].

[4] In this paper, the simulation model and plasma conditions are presented in section 2, the simulation results are described in section 3, and the discussion and conclusions are given in section 4.

2. Simulation Model

[5] A 2D electrostatic PIC code with periodic boundary conditions is employed in our simulations [*Decyk*, 1995; *Lu and Cai*, 2001]. The background magnetic field $\mathbf{B}_0$ is along the x direction. In the simulations, we only move electrons, while ions are motionless and form a neutralizing background. Initially, a potential structure, which represents an electron hole, is located in the middle of the simulation domain. The potential structure is described as

$$\phi(x) = \psi \exp\left[-0.5(x-L)^2/\Delta_\parallel^2\right], \tag{1}$$

where $\Delta_\parallel$ and L are the half width and center position of the electron hole, respectively, and ψ is the amplitude of the potential structure. The potential structure is homogeneous in the transverse direction, which is supported by a clump of trapped electrons in the electron hole. The trapped electrons gyrate in the background magnetic field and simultaneously bounce back and forth in the parallel direction of the electron hole. The motions of a trapped electron are determined by the ratio of the electron gyrofrequency Ω_e to the bounce frequency $\omega_b = \sqrt{\psi/\Delta_\parallel^2}$ [*Muschietti et al.*, 2000]. The initial electron distributions can be calculated by the BGK method self-consistently, which has already been given by *Muschietti et al.* [1999]. It is

$$F(x, v_x, v_y, v_z) = F_1(w) \exp\left[-0.5\left(v_y^2 + v_z^2\right)\Big/ T_e\right], \tag{2}$$

where T_e is the electron temperature, $w \equiv v_x^2 - 2\phi(x)$ is twice the parallel energy and

$$F_1(w) = \frac{\sqrt{-w}}{\pi\Delta_\parallel^2}\left[1 + 2\ln\left(\frac{\psi}{-2w}\right)\right] + \frac{6 + \left(\sqrt{2} + \sqrt{-w}\right)(1-w)\sqrt{-w}}{\pi\left(\sqrt{2} + \sqrt{-w}\right)(4 - 2w + w^2)}$$

$$\text{For } -2\psi \le w < 0 \tag{3a}$$

$$F_1(w) = \frac{6\sqrt{2}}{\pi(8 + w^3)} \qquad \text{For } w > 0. \tag{3b}$$

Equations (3a)) and (3b) describe the distributions of the trapped and passing electrons, respectively. The trapped electron distribution has a hollowed-out shape, while the passing electron distribution has a flat-top shape.

[6] In the simulations, the density is normalized to the unperturbed density n_0. The velocities are expressed in units of the electron thermal velocity $v_{Te} = (T_e/m_e)^{\frac{1}{2}}$. The dimensionless units used here have space in Debye length $\lambda_D = \left(\frac{\varepsilon_0 T_e}{n_0 e^2}\right)^{\frac{1}{2}}$, time in the inverse of the plasma frequency $\omega_{pe} = \left(\frac{n_0 e^2}{m_e \varepsilon_0}\right)^{1/2}$, and potential in $\frac{m_e v_{Te}^2}{e}$. Cell size unit $\lambda_D \times \lambda_D$ is used in the simulations, and the time step is $0.02\omega_{pe}^{-1}$. There are on average 625 particles in each cell, and the number of cells is 128 × 256. Initially, the electrons are loaded to satisfy equations (2) and (3).

3. Simulation Results

[7] We investigate the evolution of the perpendicular electric field in electron holes at different plasma conditions. A total of 6 runs are performed, as shown in Table 1. In runs 1–4, the initial potential is characterized by ψ = 0.8 and $\Delta_\parallel$ = 2.0, and the parameters are consistent with both the observations [*Ergun et al.*, 1998a] and the theoretical prediction [*Muschietti et al.*, 1999]. Runs 5–6, with ψ = 2.0 and $\Delta_\parallel$ = 3.0, are also performed to investigate the influence of the initial potential amplitude. However, since the two sets of hole parameters in Table 1 leave ω_b practically unchanged (with ω_b = 0.45 and 0.47, respectively), the sensitivity of the results to the value of ω_b cannot be determined from these runs.

[8] Figure 1 shows the simulation results for run 1, which correspond to weakly magnetized plasma. The bounce frequency ω_b is much smaller than the electron gyrofrequency Ω_e. In Figure 1, the top row displays the time evolution of the electric field energies E_x^2 (Figure 1a) and E_y^2 (Figure 1b), respectively, and electric field energies are normalized by $m_e^2\omega_{pe}^2 v_{Te}^2/e^2$. Below the top row of Figure 1, the left and right columns plot the electric field components E_x (Figure 1a) and E_y (Figure 1b) at $\omega_{pe}t$ = 10, 70, and 200 in the domain $32\lambda_D \le x \le 96\lambda_D$ and $0 \le y \le 128\lambda_D$. Before about $\omega_{pe}t = 30$,

Table 1. Summary of Simulations (Run 1–6)

Run Number	ψ	$\Delta_{\|}$	ω_b	Ω_e/ω_{pe}	Ω_e/ω_b
1	0.8	2.0	0.45	0.1	0.22
2	0.8	2.0	0.45	0.3	0.67
3	0.8	2.0	0.45	0.7	1.56
4	0.8	2.0	0.45	10.0	21.22
5	2.0	3.0	0.47	0.7	1.49
6	2.0	3.0	0.47	10.0	21.28

both the electric field E_x and E_y have little change. With the excitation of the transverse instability at about $\omega_{pe}t = 30$, the electric field energy E_x^2 begins to decrease and E_y^2 increases. At this point a kinked electron hole can be found in the simulation domain, and the bipolar structures of the parallel of E_y can be observed if we cut the electron hole along the direction parallel to the background magnetic field. After the transverse instability becomes sufficiently strong, it begins to destroy the electron hole. At about $\omega_{pe}t = 70$, both the electric field component E_x and E_y begin to decrease until they disappear at about $\omega_{pe}t = 150$.

[9] Figure 2 shows the simulation results for run 2, which also correspond to weakly magnetized plasma. However, the bounce frequency ω_b is comparable to the electron gyrofrequency Ω_e. The overall evolution of the electric field energies E_x^2 and E_y^2 are similar to run 1, but now the evolution is much slower because of the stabilization by the background magnetic field. The transverse instability begins to be excited at about $\omega_{pe}t = 60$ with the decrease of E_x^2 and increase of E_y^2. A kinked electron hole can be found at $\omega_{pe}t = 90$, and again we can recover the bipolar structures of the parallel cut of E_y in the electron hole. With the evolution of the electron hole, we can observe a quasi–1D electron hole from about $\omega_{pe}t = 140$, as demonstrated by *Lu et al.* [2008], during the nonlinear evolution of electron bistream instabilities implemented with 2D PIC simulations. In a quasi–1D electron hole, along the direction perpendicular to the background magnetic field, a variation for E_x can be found, while for E_y a series of islands (with alternate positive and negative E_y) are formed. Therefore, the unipolar structures of the parallel cut of E_y can be found in the electron hole, which is caused by the combined actions

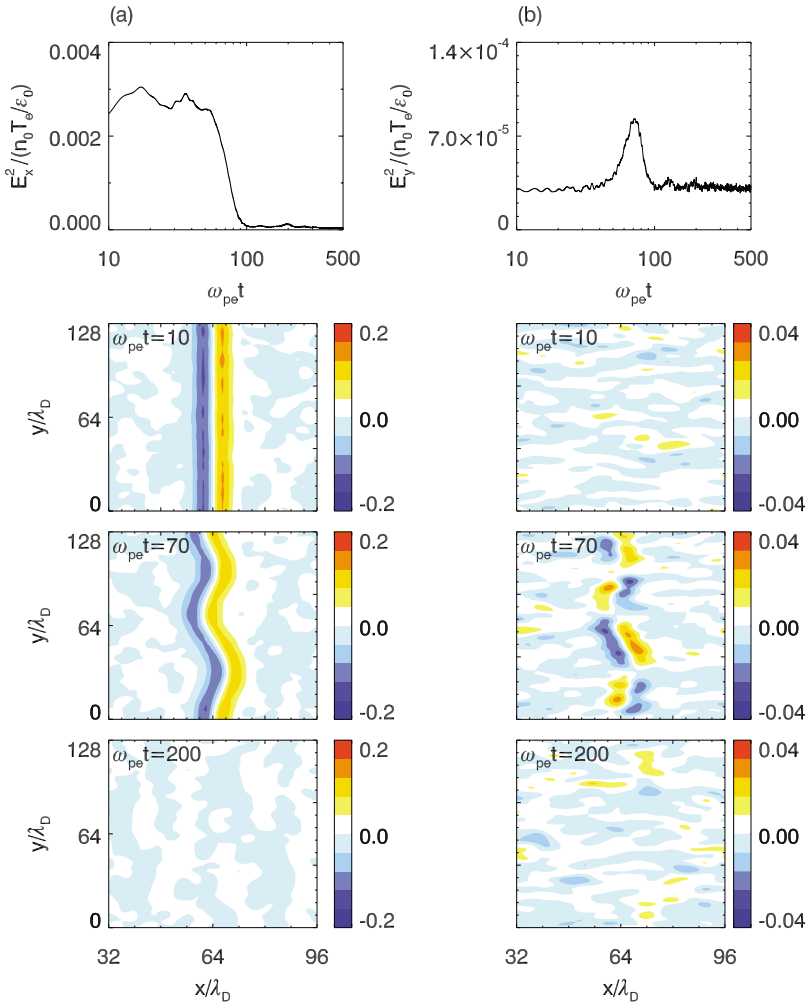

Figure 1. The top row shows the time evolution of the electric field energies (a) E_x^2 and (b) E_y^2, respectively, normalized by $m_e^2\omega_{pe}^2v_{Te}^2/e^2$. Below the top row, the left and right columns plot the electric field component Figure 1a E_x and Figure 1b E_y at $\omega_{pe}t$ = 10, 70, and 200 for run 1 in the domain $32\lambda_D \le x \le 96\lambda_D$ and $0 \le y \le 128\lambda_D$.

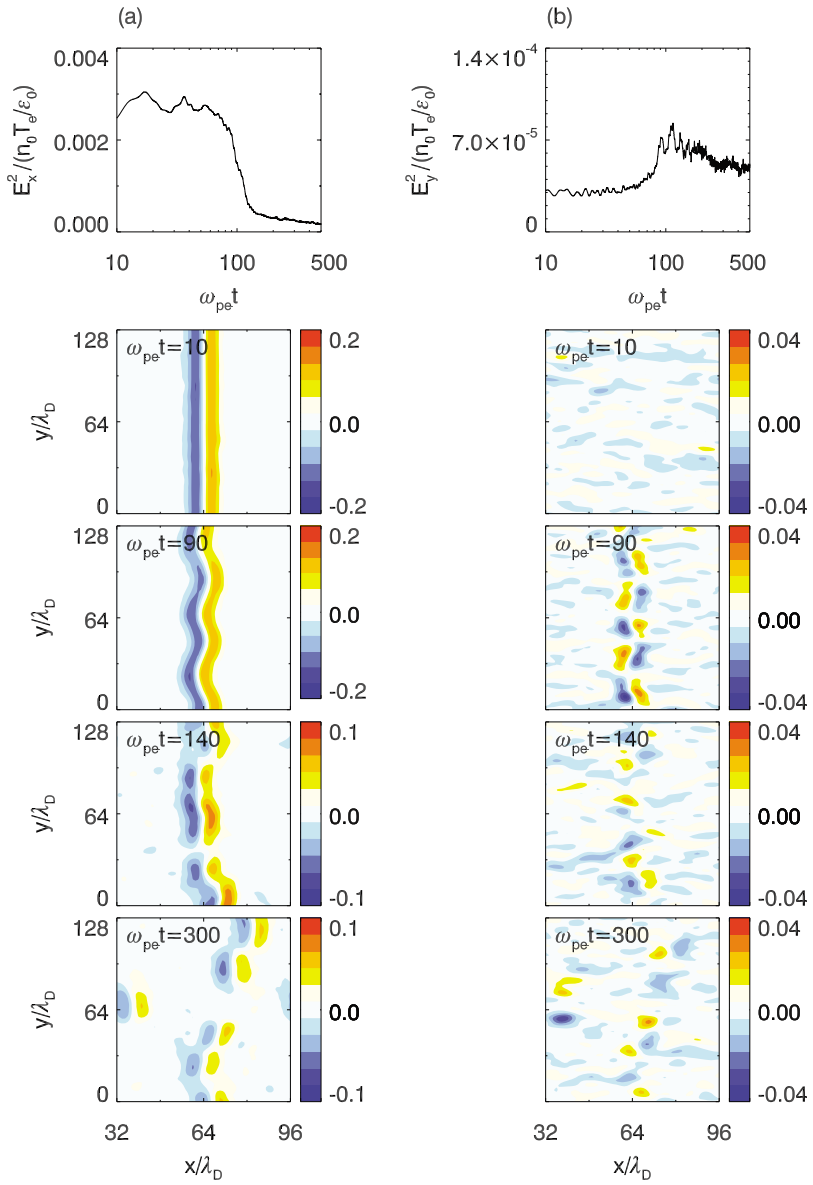

Figure 2. The top row shows the time evolution of the electric field energies (a) E_x^2 and (b) E_y^2, respectively, normalized by $m_e^2\omega_{pe}^2 v_{Te}^2/e^2$. Below the top row, the left and right columns plot the electric field component Figure 2a E_x and Figure 2b E_y at $\omega_{pe}t$ = 10, 90, 140, and 300 for run 2 in the domain $32\lambda_D \le x \le 96\lambda_D$ and $0 \le y \le 128\lambda_D$.

between the transverse instability and the stabilization by the background magnetic field. When the transverse instability is sufficiently strong, it begins to destroy the electron hole at about $\omega_{pe}t = 240$. At first, the electron hole begins to be broken into several segments, and several 2D electron holes which are isolated in both the x and y directions are formed. In the 2D dimensional electron holes, the parallel cut of E_y also has unipolar structure. As time goes on, such 2D electron holes become weaker and weaker until they disappear at about $\omega_{pe}t$ = 1700. In this run, the bipolar and unipolar structures of E_y can persist for about 100 and 1000 plasma periods, respectively.

[10] Figure 3 shows the simulation results for run 3, where the electron gyrofrequency Ω_e is larger than the bounce frequency ω_b. Although the evolution is similar to run 2, the decay of the electron hole is much slower. In summary, a kinked electron hole with a bipolar structure of the parallel cut of E_y is formed at about $\omega_{pe}t = 100$. At about $\omega_{pe}t = 700$, a quasi–1D electron hole is formed, and the parallel cut of E_y has a unipolar structure in the electron hole.

[11] Figure 4 plots the simulation results for run 4, which correspond to strongly magnetized plasma, and the electron gyrofrequency Ω_e is much larger than the bounce frequency ω_b. The evolution is similar to runs 2 and 3, however, here a quasi–1D electron hole with unipolar structures of E_y can persist for a much longer time. We can still find the existence of a quasi–1D electron hole until the end of the run (at about $\omega_{pe}t$ = 4500). Therefore, the lifetime of the unipolar structures of E_y is several thousands of plasma periods.

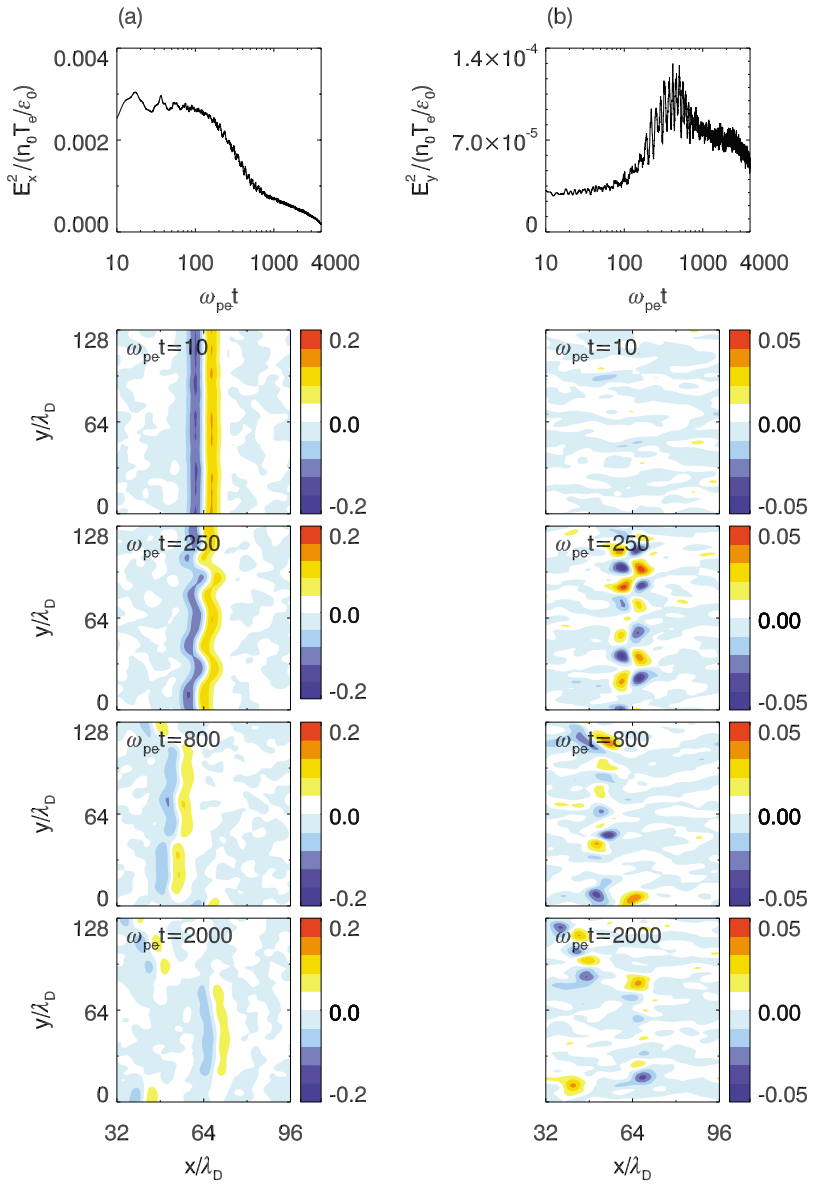

Figure 3. The top row shows the time evolution of the electric field energies (a) E_x^2 and (b) E_y^2, respectively, normalized by $m_e^2\omega_{pe}^2v_{Te}^2/e^2$. Below the top row, the left and right columns plot the electric field component Figure 3a E_x and Figure 3b E_y at $\omega_{pe}t$ = 10, 250, 800, and 2000 for run 3 in the domain $32\lambda_D \le x \le 96\lambda_D$ and $0 \le y \le 128\lambda_D$.

[12] We also investigate the influences of the initial potential amplitude ψ on the evolution of the electron hole. The simulation results for run 5, shown in Figure 5, correspond to weakly magnetized plasma. The electron gyrofrequency Ω_e is larger than the bounce frequency ω_b. The evolution of the electron hole is similar to run 3. At about $\omega_{pe}t$ = 380, the transverse instability begins to be excited, and a kinked electron hole with a bipolar structure of the parallel cut of E_y is formed. A quasi–1D electron hole with a unipolar structure of E_y is formed at about $\omega_{pe}t$ = 800; the electron hole then decays into several 2D segments. The difference is that the transverse instability excites electrostatic whistler waves with streaked structures for E_y outside of the electron hole. The electrostatic whistler waves are also often observed in the multidimensional PIC simulations of electron bistream instabilities [*Goldman et al.*, 1999; *Oppenheim et al.*, 1999; *Lu et al.*, 2008]. The electrostatic whistlers become weaker with the decay of the electron hole into several 2D segments. Figure 6 plots the simulation results for run 6, which correspond to strongly magnetized plasma, and the electron gyrofrequency Ω_e is much larger than the bounce frequency ω_b. The evolution of the electron hole is similar to run 5. However, in run 6 the electrostatic whistler waves are much stronger. Both the electrostatic whistler waves and the quasi–1D electron hole with unipolar structures of E_y persist until the end of the run.

[13] The evolution of the electron holes at different plasma conditions can be explained on the basis of the interactions between the transverse instability and stabilization by the background magnetic field, as demonstrated by *Muschietti*

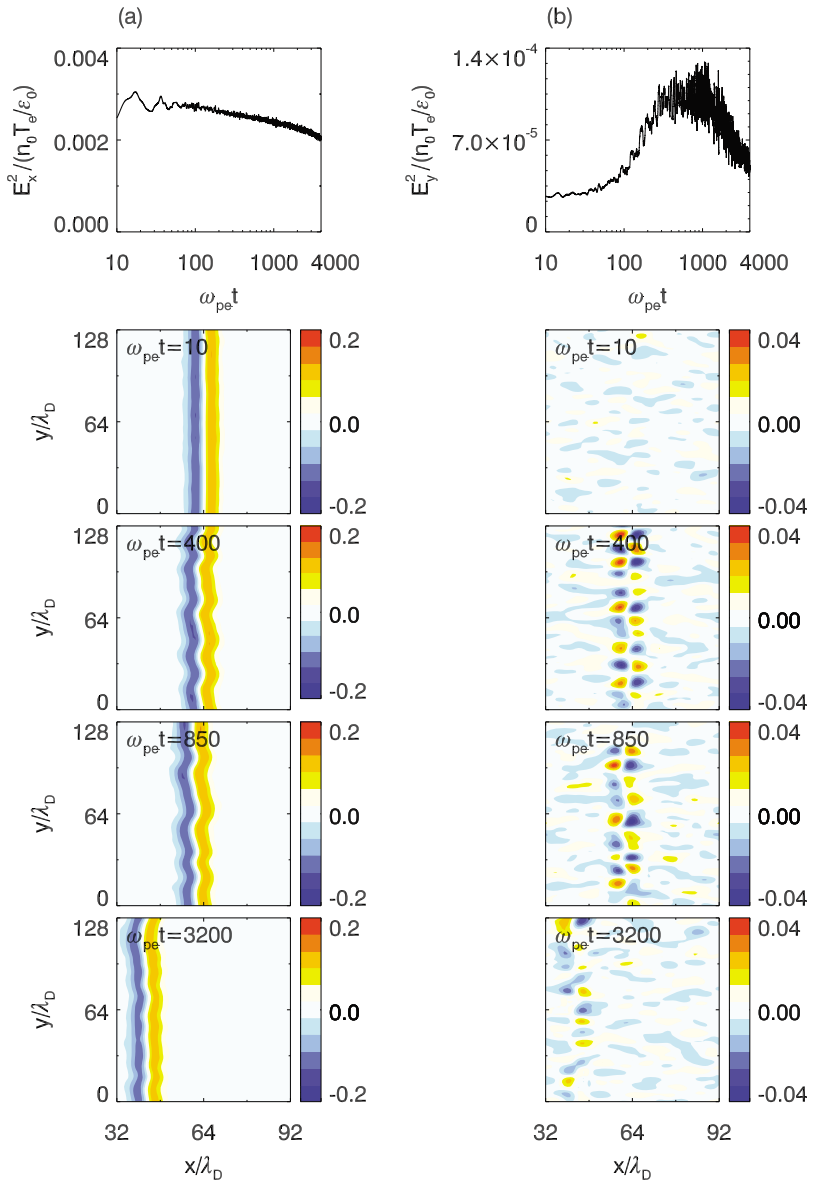

Figure 4. The top row shows the time evolution of the electric field energies (a) E_x^2 and (b) E_y^2, respectively, normalized by $m_e^2\omega_{pe}^2 v_{Te}^2/e^2$. Below the top row, the left and right columns plot the electric field component Figure 4a E_x and Figure 4b E_y at $\omega_{pe}t$ = 10, 400, 850, and 3200 for run 4 in the domain $32\lambda_D \le x \le 96\lambda_D$ and $0 \le y \le 128\lambda_D$.

et al. [2000], and confirmed by *Lu et al.* [2008]. The transverse instability is a self-focusing type of instability acting at the level of the particle trajectories [*Muschietti et al.*, 2000]. This can be illustrated by following electron trajectories in a kinked electron hole, whose potential is modeled as [*Muschietti et al.*, 2000]

$$\phi(x,y) = \psi \exp\left[-0.5\left(\frac{x - 32.0 - \varepsilon\Delta_{\|}\cos ky}{\Delta_{\|}}\right)^2\right], \qquad (4)$$

where ε is a measure of the perturbation and k is its transverse wave number. The parameters are $\psi = 2.0$, $\Delta_{\|} = 3.0$, $\varepsilon = 0.5$ and $k = 0.22$. Figure 7 shows the contours of the charge density ρ, the electric field E_x, and the electric field E_y, which are calculated on the basis of equation (4). In the electron hole, the charge density changes along the y direction, and the parallel cut of E_y has bipolar structures. Typical electron trajectories are plotted in Figure 8. Figure 8a shows electrons trapped in an electron hole, and Figure 8b shows electrons passing through an electron hole. Initially, these electrons are distributed evenly in the y direction, and in the x direction they start from $x = 28\lambda_D$ in Figure 8a and $x = 11\lambda_D$ in Figure 8b. The background magnetic field is $B_0 = 0.7$, and the charge density is also plotted. The trapped electrons tend to accumulate to the regions that already have a surplus of electrons (with negative charge density). The transverse undulation in the electron hole then becomes more and more pronounced, which results in a self-focusing type of instability. The electrons passing through the electron hole also

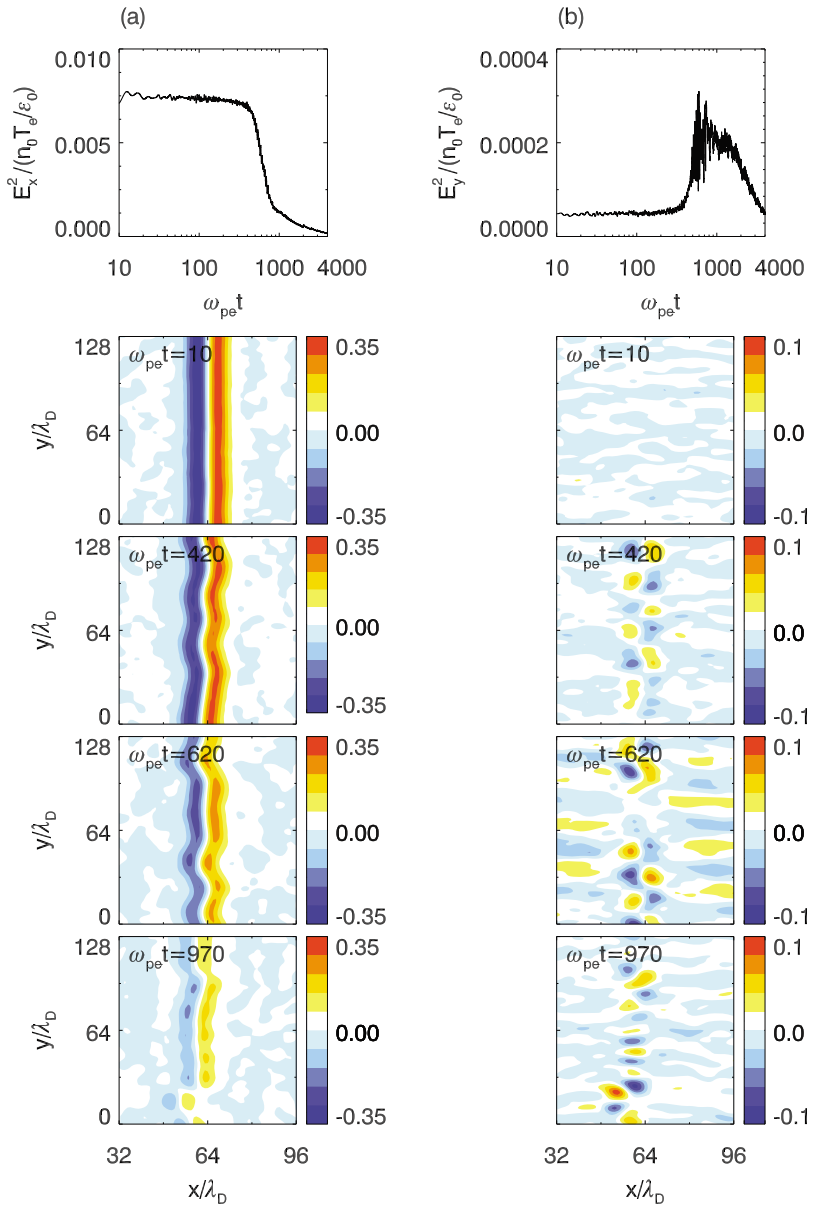

Figure 5. The top row shows the time evolution of the electric field energies (a) E_x^2 and (b) E_y^2, respectively, normalized by $m_e^2\omega_{pe}^2v_{Te}^2/e^2$. Below the top row, the left and right columns plot the electric field component Figure 5a E_x and Figure 5b E_y at $\omega_{pe}t$ = 10, 420, 620, and 970 for run 5 in the domain $32\lambda_D \le x \le 96\lambda_D$ and $32\lambda_D \le x \le 96\lambda_D$.

tend to accumulate to some regions, with the charge density changing along the y direction. This leads to the streaked structures of E_y outside of the electron hole.

[14] Figure 9 shows the contours of charge density ρ at $\omega_{pe}t$ = 970 for run 6. Here, we choose run 6 with the background magnetic field B_0 = 10 because in run 5 the kinked electron hole decays so fast that there is no sufficient time to form strong electrostatic whistler waves. The charge density inside and outside of the electron hole changes along the y direction, forming structures which exactly match the prediction in Figure 8. The streaked structures of E_y outside of the electron holes can be explained by the variations of the charge density along the y direction in the corresponding regions. The variations of the charge density at $x = 28\lambda_D$ outside of the electron holes are shown in Figure 10, and $\partial E_y/\partial y$ is also plotted. We can find $\partial E_y/\partial y \approx \rho$. Therefore, the variations of ρ along the y direction lead to the corresponding variations of $\partial E_y/\partial y$ outside of the electron holes, producing regular streaked structures of E_y along the y direction. Subsequently the interactions between the streaked structures of E_y and the vibrations of the kinked electron hole emit electrostatic whistler waves. The electrostatic whistler waves propagate along the direction nearly perpendicular to the ambient magnetic field. The propagating direction and frequency of the electrostatic whistler waves are consistent with the theoretical results [*Vetoulis and Oppenheim*, 2001; *Jovanovic and Schamel*, 2002]. Such a process of emitting electrostatic whistler waves can be demonstrated in Figure 11,

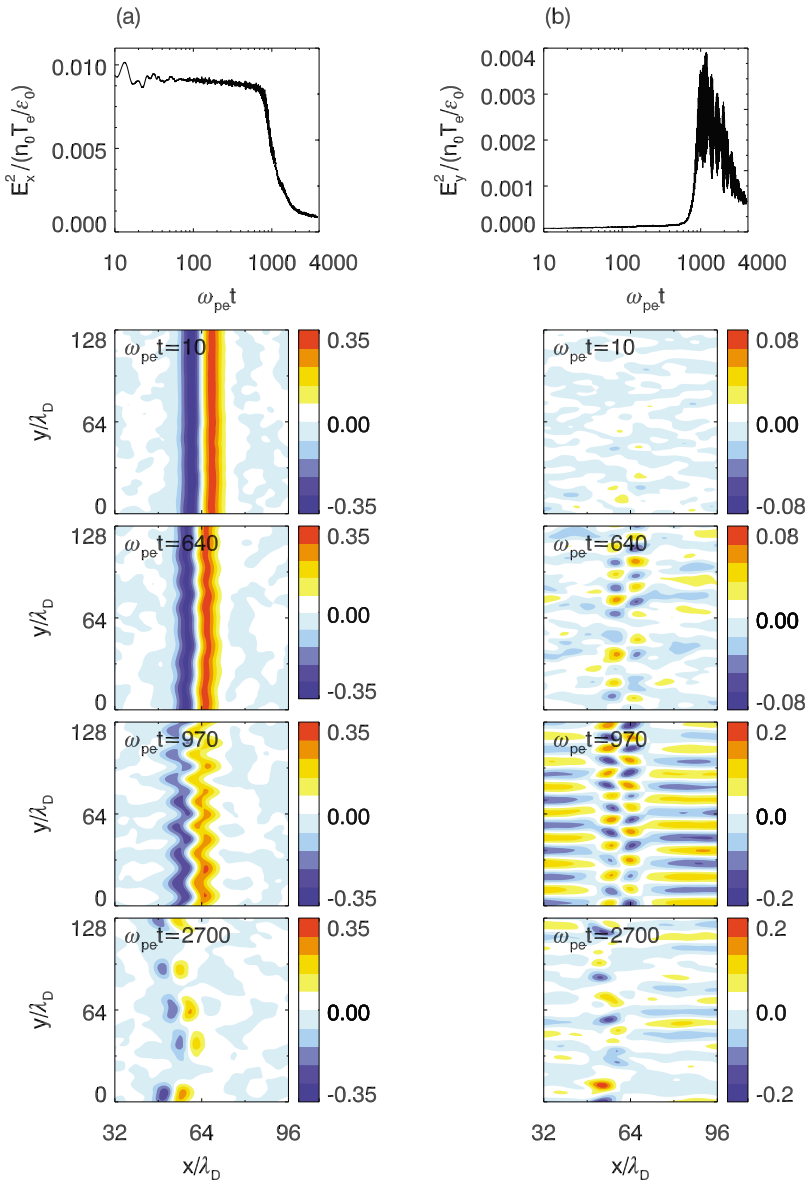

Figure 6. The top row shows the time evolution of the electric field energies (a) E_x^2 and (b) E_y^2, respectively, normalized by $m_e^2\omega_{pe}^2v_{Te}^2/e^2$. Below the top row, the left and right columns plot the electric field component Figure 6a E_x and Figure 6b E_y at $\omega_{pe}t$ = 10, 640, 970, and 2700 for run 6 in the domain $32\lambda_D \le x \le 96\lambda_D$ and $0 \le y \le 128\lambda_D$.

which shows the frequency spectra of E_y inside and outside of the electron hole. The variations of E_y inside the electron hole are caused by the vibrations of the kinked electron hole. The spectrum of E_y outside of the electron hole is similar to that inside the electron hole, and the frequencies are concentrated at around $0.15\omega_{pe}$. Therefore, we can conclude that electrons passing through the electron hole lead to the variations of ρ and then E_y along the y direction outside of the electron holes. When this occurs, the interactions between the streaked structures of E_y and the vibrating kinked electron hole emit electrostatic whistler waves.

[15] The magnetic field guides the trapped electrons that bounce back and forth in electron holes. This prevents the trapped electrons from being focused by the transverse gradients of the potential, thereby making the electron hole stable. As the background magnetic field increases, the process of self-focusing becomes slower, and more time is needed to form the bipolar and unipolar structures of E_y in the electron holes. The increase of the background magnetic field also causes the gyro-radii of the trapped electrons to become smaller. These electrons tend to stay in their original positions, and therefore the wave number k of the transverse instability in the kinked electron holes becomes larger. This can be demonstrated in Figure 12, which plots the ratio $\Delta_{\|}/\Delta_{\perp}$ of the kinked electron holes at different background magnetic field levels. Here we define $\Delta_{\perp}$ as 0.25 times the wavelength of the transverse instability, which can also be regarded as the perpendicular-scale size of the electron holes calculated from the self-consistent PIC simulations when the kinked electron holes are fully developed. The

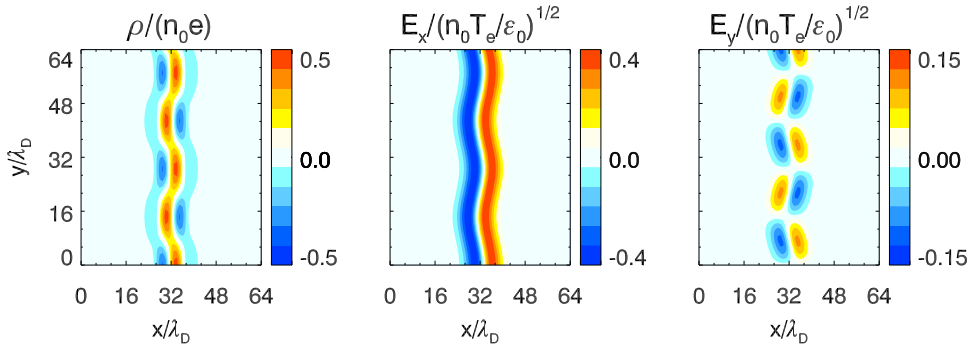

Figure 7. The contours of (a) the charge density ρ, (b) the electric field component E_x, and (c) the electric field component E_y, which is calculated on the basis of equation (4).

$\Delta_\parallel/\Delta_\perp$ increases rapidly from 0.28 around $B_0 = 0.3$ to 0.8 around $B_0 = 2.0$. We can also find two particle limiting values for $\Delta_\parallel/\Delta_\perp$, 0.16 when the magnetic field is sufficiently weak, and 0.8 when it is sufficiently strong. Additional runs were performed with the same parameters except for the extended simulation domain in the y direction to $512\lambda_D$, yielding almost identical values for $\Delta_\parallel/\Delta_\perp$. Therefore, we can conclude that the two particular limiting values are physical, not numerical results.

[16] The two particular limiting values can be explained as follows: in very weakly magnetized plasma, the effect of the magnetic field is negligible. As pointed out in *Muschietti et al.* [2000], the wave number k is determined by only the bounce frequency ω_b and the thermal velocity. Therefore, $\Delta_\parallel/\Delta_\perp \sim \sqrt{\psi}/v_e$, and it is independent of the magnetic field. In strongly magnetic plasma, assuming that the transverse and parallel derivatives in the Poisson equation are in approximate balance after the gyrophase-averaged distribution function is utilized, [*Franz et al.*, 2000], the wave number can be expressed as

$$\frac{\Delta_\parallel}{\Delta_\perp} \sim \left(1 + \frac{\omega_{pe}^2}{\Omega_e^2}\right)^{-1/2}. \quad (5)$$

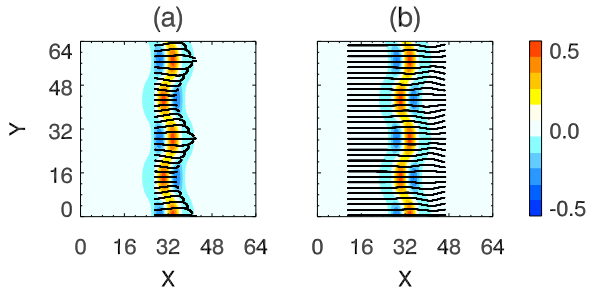

Figure 8. The trajectories of typical electrons: (a) electrons trapped in the electron holes, and (b) electrons passing through the electron holes. In the figure, contours of the charge density ρ, calculated on the basis of equation (4), is also plotted. Initially, these electrons are distributed evenly in the y direction, starting from $x = 28\lambda_D$ for Figure 8a and $x = 11\lambda_D$ for Figure 8b. The background magnetic field is $B_0 = 0.7$.

When the magnetic field is sufficiently strong, $\Delta_\parallel/\Delta_\perp$ is independent of the magnetic field.

4. Discussion and Conclusions

[17] By performing 2D electrostatic PIC simulations, we investigate the evolution of electron holes at different plasma conditions, with an emphasis on the structure of the perpendicular electric field inside and outside of the electron holes. Our results show that the transverse instability causes the decay of electron holes, while the background magnetic field tends to stabilize it. Their combined actions determine the evolution of the electron holes. The transverse instability causes the electron holes become kinked, and the parallel cut of $E_\perp$ in the electron holes has bipolar structures. However, in very weakly magnetized plasma ($\Omega_e \ll \omega_{pe}$), the kinked electron holes decay very fast and last for only tens of electron plasma periods. With the increase of the background magnetic field, the evolution of the electron holes becomes slower. The bipolar structures of the parallel cut of $E_\perp$ in the electron holes can evolve into unipolar structures. In very strongly magnetized plasma ($\Omega_e \gg \omega_{pe}$), when the initial potential amplitude ψ of the electron hole is sufficiently strong, streaked structures of $E_\perp$ can be formed

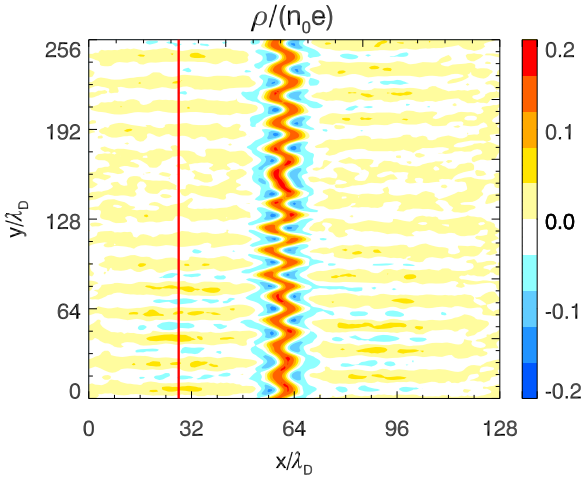

Figure 9. The charge density ρ, normalized by $n_0 e$ at $\omega_{pe}t = 970$ for run 6. The the red line indicates the x location of the cut shown in Figure 10.

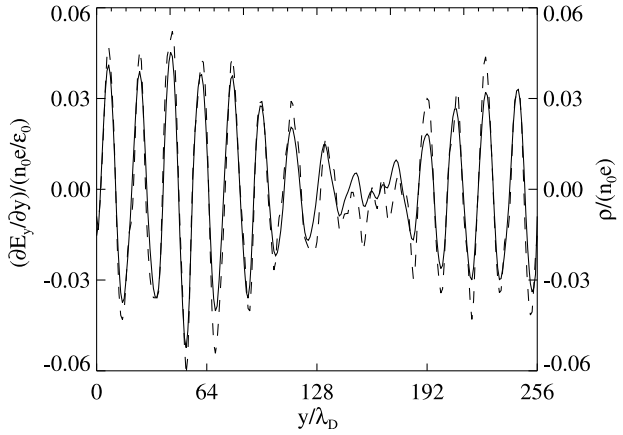

Figure 10. The perpendicular cut of charge density ρ and $\partial E_y/\partial y$ along $x = 28\lambda_D$ (as indicated by the red line in Figure 9) at $\omega_{pe}t = 970$ for run 6. The solid and dashed lines denote $\partial E_y/\partial y$ and ρ, respectively.

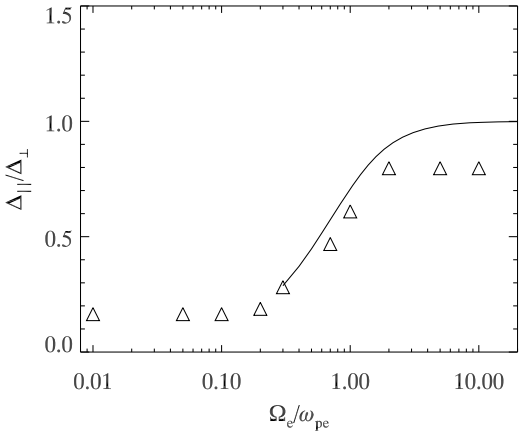

Figure 12. The value of $\Delta_\parallel/\Delta_\perp$ in the kinked electron holes at different background magnetic fields for $\psi = 0.8$ and $\Delta_\parallel = 2.0$. The perpendicular scale sizes $\Delta_\perp$ are calculated from the self-consistent PIC simulations without initial perturbations when the kinked electron holes are fully developed. The triangle denotes the results obtained from the simulation, and the solid line describes the results based on equation (5) for $\Omega_e/\omega_{pe} > 0.3$.

outside of the electron holes. When this occurs, the interactions between the streaked structures of $E_\perp$ and the vibrations of the kinked electron hole emit electrostatic whistler waves.

[18] The unipolar structures of the parallel cut of $E_\perp$ have been observed by the FAST satellite in the auroral region [*Ergun et al.*, 1998a, 1998b]. Consistent with these space observations, our present simulations also revealed that the parallel cut of the perpendicular electric field $E_\perp$ has unipolar structures. The generation mechanism of such structures is governed by the interactions between the transverse instability and stabilization by the background magnetic field. The structures are shown to last for thousands of electron plasma periods in strongly magnetized plasma. These results provide a possible explanation for the unipolar structures of the parallel cut of $E_\perp$ observed in the auroral region where plasma is strongly magnetized. In our simulations, we also find the two particular limiting values for $\Delta_\parallel/\Delta_\perp$ when the magnetic field is sufficiently strong and weak, which is consistent with the Polar satellite observations examined by *Franz et al.* [2000]. The particular limiting value for $\Delta_\parallel/\Delta_\perp$ when the magnetic field is sufficiently strong has been theoretically explained in *Franz et al.* [2000]. On the basis of the theory of the transverse instability, we predict that there is still another particular limiting value for $\Delta_\parallel/\Delta_\perp$ when the magnetic field is sufficiently weak, which is also consistent with the observations in *Franz et al.* [2000] (see Figure 3).

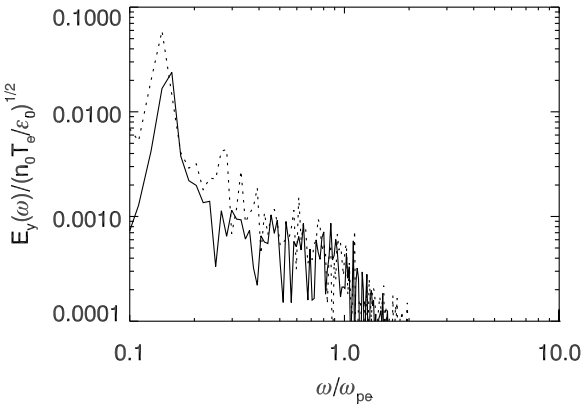

Figure 11. The frequency spectra of E_y inside and outside of the electron hole during the time period $\omega_{pe}t = 900 \sim 1300$ for run 6. The dashed line is obtained by Fourier transform E_y inside electron holes ($x = 61\lambda_D$, $y = 64\lambda_D$), and the solid line is obtained by Fourier transform E_y outside electron holes ($x = 32\lambda_D$, $y = 64\lambda_D$).

[19] The perpendicular electric field in the electron holes will also influence the electron trajectories which pass through the holes. This leads to the variation of the charge density ρ along the y direction, which forms the streaked structures of $E_\perp$ outside the electron holes. When this occurs, the interactions between the streaked structures of $E_\perp$ and the vibrations of the kinked electron hole emit electrostatic whistler waves. Electrostatic whistler waves are often observed in 2D simulations of electron bistream instabilities. Several mechanisms, including (1) the bounce motion of trapped electrons in electron holes [*Oppenheim et al.*, 2001; *Berthomier et al.*, 2002] and (2) the vibration of kinked electron holes [*Newman et al.*, 2001b] have been proposed to explain the emission of the electrostatic whistler waves. Our simulations seem to indicate that the probable mechanism is vibration of kinked electron holes.

[20] **Acknowledgments.** This research was supported by the National Science Foundation of China (NSFC) under grants 40974081, 40725013, 40931053, Chinese Academy of Sciences grant KJCX2-YW-N28, and the Specialized Research Fund for State Key Laboratories.

[21] Philippa Browning thanks the reviewers for their assistance in evaluating this paper.

References

Amano, T., and M. Hoshino (2009), Nonlinear evolution of Buneman instability and its implication for electron acceleration in high Mach number collisionless perpendicular shocks, *Phys. Plasmas*, *16*, 102901.

Bale, S. D., P. J. Kellogg, D. E. Larson, R. P. Lin, K. Gpetz, and R. P. Lepping (1998), Bipolar electrostatic structures in the shock transition region: Evidence of electron phase holes, *Geophys. Res. Lett.*, *25*, 2929–2932, doi:10.1029/98GL02111.

Bernstein, I. B., J. M. Greene, and M. D. Kruskal (1957), Exact nonlinear plasma oscillations, *Phys. Rev.*, *108*, 546–550.

Berthomier, M., L. Muschietti, J. W. Bonnell, I. Roth, and C. W. Carlson (2002), Interaction between electrostatic whistlers and electron holes in the auroral region, *J. Geophys. Res.*, *107*(A12), 1463, doi:10.1029/2002JA009303.

Bret, A., M. E. Dieckmann, and C. Deutsch (2006), Oblique electromagnetic instabilities for a hot relativistic beam interacting with a hot and magnetized plasma, *Phys. Plasmas*, *13*, 082109.

Cattell, C., J. Crumley, J. Dombeck, J. Wygant, and F. S. Mozer (2002), Polar observations of solitary waves at Earth's magnetopause, *Geophys. Res. Lett.*, *29*(5), 1065, doi:10.1029/2001GL014046.

Chen, L. J., J. Pickett, P. Kintner, J. Franz, and D. Gurnett (2005), On the width-amplitude inequality of electron phase-space holes, *J. Geophys. Res.*, *110*, A09211, doi:10.1029/2005JA011087.

Decyk, V. K. (1995), Skeleton PIC codes for parallel computers, *Comput. Phys. Commun.*, *87*, 87–94.

Ergun, R. E., C. W. Carlson, J. P. McFadden, and F. S. Mozer (1998a), Fast satellite observations of large-amplitude solitary structures, *Geophys. Res. Lett.*, *25*(12), 2041–2044, doi:10.1029/98GL00636.

Ergun, R. E., C. W. Carlson, J. P. McFadden, F. S. Mozer, L. Muschietti, I. Roth, and R. J. Strangeway (1998b), Debye-Scale plasma structures associated with magnetic-field-aligned electric fields, *Phys. Res. Lett.*, *81*, 826–829.

Franz, J. R., P. M. Kintner, and J. S. Pickett (1998), POLAR observations of coherent electric field structures, *Geophys. Res. Lett.*, *25*(8), 1277–1280, doi:10.1029/98GL50870.

Franz, J. R., P. M. Kintner, C. E. Seyler, J. S. Pickett, and J. D. Scudder (2000), On the perpendicular scale of electron phase-space holes, *Geophys. Res. Lett.*, *27*(2), 169–172, doi:10.1029/1999GL010733.

Franz, J. R., P. M. Kintner, J. S. Pickett, and L. J. Chen (2005), Properties of small-amplitude electron phase-space holes observed by Polar, *J. Geophys. Res.*, *110*, A09212, doi:10.1029/2005JA011095.

Goldman, M. V., M. M. Oppenheim, and D. L. Newman (1999), Nonlinear two-stream instabilities as an explanation for auroral bipolar wave structures, *Geophys. Res. Lett.*, *26*(13), 1821–1824, doi:10.1029/1999GL900435.

Grabbe, C. L., and J. D. Menietti (2006), Broadband electrostatic wave observations in the auroral region on Polar and comparsions with theory, *J. Geophys. Res.*, *111*, A10226, doi:10.1029/2006JA011602.

Jovanovic, D., and H. Schamel (2002), The stability of propagating slab electron holes in a magnetized plasma, *Phys. Plasmas*, *9*, 5079–5087

Lu, Q. M., and D. S. Cai (2001), Implementation of parallel plasma particle-in-cell codes on PC cluster, *Comput. Phys. Commun.*, *135*, 93–104.

Lu, Q. M., D. Y. Wang, and S. Wang (2005a), Generation mechanism of electrostatic solitary waves in the Earth's auroral region, *J. Geophys. Res.*, *110*, A03223, doi:10.1029/2004JA010739.

Lu, Q. M., S. Wang, and X. K. Dou (2005b), Electrostatic waves in an electron-beam plasma system, *Phys. Plasmas*, *12*, 072903.

Lu, Q. M., B. Lembege, J. B. Tao, and S. Wang (2008), Perpendicular electric field in two-dimensional electron phase-holes: A parameter study, *J. Geophys. Res.*, *113*, A11219, doi:10.1029/2008JA013693.

Mangeney, A., C. Salem, C. Lacombe, J. L. Bougeret, C. Perche, R. Manning, P. J. Kellogg, K. Goetz, S. J. Monson, and J. M. Bosqued (1999), WIND observations of coherent electrostatic waves in the solar wind, *Ann. Geophys.*, *17*, 307–320.

Matsumoto, H., H. Kojima, T. Miyatake, Y. Omura, M. Okada, I. Nagano, and M. Tsutsui (1994), Electrostatic solitary waves (ESW) in the magnetotail: BEN wave forms observed by Geotail, *Geophys. Res. Lett.*, *21*(25), 2915–2918, doi:10.1029/94GL01284.

Morse, R. L., and C. W. Nielson (1969), One-, two-, and three-dimensional numerical simulation of two-beam plasmas, *Phys. Rev. Lett.*, *23*, 1087–1089.

Mottez, F., S. Perraut, A. Roux, and P. Louarn (1997), Coherent structures in the magnetotail triggered by counterstreaming electron beams, *J. Geophys. Res.*, *102*(A6), 11,399–11,408, doi:10.1029/97JA00385.

Muschietti, L., R. E. Ergun, I. Roth, and C. W. Carlson (1999), Phase-space electron holes along magnetic field lines, *Geophys. Res. Lett.*, *26*(8), 1093–1096, doi:10.1029/1999GL900207.

Muschietti, L., I. Roth, C. W. Carlson, and R. E. Ergun (2000), Transverse instability of magnetized electron holes, *Phys. Rev. Lett.*, *85*, 94–97.

Newman, D. L., M. V. Goldman, R. E. Ergun, and A. Mangeney (2001a), Formation of double layers and electron holes in a current-driven space plasma, *Phys. Rev. Lett.*, *87*, 255001.

Newman, D. L., M. V. Goldman, M. Spector, and F. Perez (2001b), Dynamics and instability of electron phase-space tubes, *Phys. Rev. Lett.*, *86*, 1239–1242.

Ng, C. S., and A. Bhattacharjee (2005), Bernstein-Greene-Kruskal modes in a three-dimensional plasma, *Phys. Rev. Lett.*, *95*, 245004.

Omura, Y., H. Kojama, and H. Matsumoto (1994), Computer simulation of electrostatic solitary waves: A nonlinear model of broadband electrostatic noise, *Geophys. Res. Lett.*, *21*(25), 2923–2926, doi:10.1029/94GL01605.

Oppenheim, M., D. L. Newman, and M. V. Goldman (1999), Evolution of electron phase-space holes in a 2D magnetized plasma, *Phys. Rev. Lett.*, *83*, 2344–2347.

Oppenheim, M., G. Vetoulis, D. L. Newman, and M. V. Goldman (2001), Evolution of electron phase-space holes in 3D, *Geophys. Res. Lett.*, *28*(9), 1891–1894, doi:10.1029/2000GL012383.

Pickett, J. S., L. J. Chen, S. W. Kahler, O. Santolik, D. A. Gurnett, B. T. Tsurutani, and A. Balogh (2004), Isolated electrostatic structures observed throughout the cluster orbit: Relationship to magnetic field strength, *Ann. Geophys.*, *22*, 2525–2523.

Roberts, K. V., and H. L. Berks (1967), Nonlinear evolution of a two-stream instability, *Phys. Rev. Lett.*, *19*, 297–300.

Saeki, K., P. Michelsen, H. L. Pecseli, and J. J. Rasmussen (1979), Formation and coalescence of electron solitary holes, *Phys. Rev. Lett.*, *42*, 501–504.

Sarri, G., M. E. Dieckmann, et al. (2010), Observation and characterization of laser-driven phase space electron holes, *Phys. Plasmas*, *17*, 010701.

Vetoulis, G., and M. Oppenheim (2001), Electrostatic mode excitation in electron holes due to wave bounce resonances, *Phys. Rev. Lett.*, *86*, 1235–1238.

C. Huang, Q. Lu, S. Wang, and M. Wu, CAS Key Laboratory of Basic Plasma Physics, School of Earth and Space Sciences, University of Science and Technology of China, Hefei, Anhui 230026, China. (qmlu@ustc.edu.cn)